Geophysical Journal International

Geophys. J. Int. (2021) **224,** 1116–1126
Advance Access publication 2020 October 27
GJI Geomagnetism, Rock Magnetism and Palaeomagnetism

doi: 10.1093/gji/ggaa514

Experimental test of the cooling rate effect on blocking temperatures in stepwise thermal demagnetization

Thomas A. Berndt [1], Liao Chang,[2] Greig A. Paterson [3,4] and Changqian Cao[4,5]

[1] *Department of Geophysics, School of Earth and Space Sciences, Peking University, Beijing* 100871, *P. R. China. E-mail: thomasberndt@pku.edu.cn*
[2] *Laboratory of Orogenic Belts and Crustal Evolution, School of Earth and Space Sciences, Peking University, Beijing* 100871, *P. R. China*
[3] *Department of Earth, Ocean and Ecological Sciences, University of Liverpool, Liverpool, L697ZE, UK*
[4] *Biogeomagnetism Group, Paleomagnetism and Geochronology Laboratory, Key Laboratory of Earth and Planetary Physics, Institute of Geology and Geophysics, Chinese Academy of Sciences, Beijing* 100029, *China*
[5] *Innovation Academy for Earth Science, Chinese Academy of Sciences, Beijing 100029, China*

Accepted 2020 October 23. Received 2020 September 28; in original form 2020 May 5

SUMMARY

Upon cooling, most rocks acquire a thermoremanent magnetization (TRM); the cooling rate at which this happens not only affects palaeointensity estimates, but also their unblocking temperatures in stepwise thermal demagnetization experiments, which is important, for example, to estimate volcanic emplacement temperatures. Traditional single-domain (SD) theory of magnetic remanence relates relaxation times to blocking temperatures— the blocking temperature is the temperature at which the relaxation time becomes shorter than the experimental timescale—and therefore strictly only applies to remanence acquisition mechanisms at constant temperatures (i.e. viscous remanent magnetizations, VRMs). A theoretical framework to relate (constant) blocking temperatures to (time-varying) cooling rates exists, but this theory has very limited experimental verification—partly due to the difficulty of accurately knowing the cooling rates of geological materials. Here we present an experimental test of this 'cooling rate effect on blocking temperatures' through a series of demagnetization experiments of laboratory-induced TRMs with controlled cooling rates. The tested cooling rates span about 1 order of magnitude and are made possible through (1) extremely accurate demagnetization experiments using a low-temperature magnetic properties measurement system (MPMS) and (2) the use of a '1-step-only' stepwise thermal demagnetization protocol where the relaxation process is measured over time. In this way the relaxation time corresponding to the blocking temperature is measured, which can be done to much higher accuracy than measuring the blocking temperature directly as done in traditional stepwise thermal demagnetization experiments. Our experiments confirm that the cooling rate relationship holds to high accuracy for ideal magnetic recorders, as shown for a synthetic weakly interacting SD magnetoferritin sample. A SD-dominated low-Ti titanomagnetite Tiva Canyon Tuff sample, however, showed that natural samples are unlikely to be sufficiently 'ideal' to meet the theoretical predictions to high accuracy—the experimental data agrees only approximately with the theoretical predictions, which may potentially affect blocking temperature estimates in stepwise thermal demagnetization experiments. Moreover, we find a strongly enhanced cooling rate effect on palaeointensities for even marginally non-ideal samples (up to 43 per cent increase in pTRM for a halving of the cooling rate).

Key words: Magnetic mineralogy and petrology; Palaeointensity; Palaeomagnetism; Remagnetization; Rock and mineral magnetism.

1 INTRODUCTION

Most igneous rocks contain ferromagnetic minerals that, upon cooling, acquire a thermoremanent magnetization (TRM, see Table A1 for a list of acronyms) aligned with the Earth's ambient magnetic field. Subsequently, these rocks may acquire overprints of partial TRMs (pTRM) due to reheating, or of viscous remanent magnetizations (VRM) due to exposure to magnetic fields over very long times. The temperatures at which VRMs/TRMs are acquired (blocking temperature) T_A play an important role, for example, to

determine emplacement temperatures (McClelland & Druitt 1989; Paterson *et al.* 2010b) and for viscous remanent magnetizations (VRM) dating (Heller & Markert 1973; Sato *et al.* 2014; Berndt & Muxworthy 2017). The different natural remanent magnetization (NRM) components can be isolated in thermal demagnetization experiments, during which the sample is heated to successively higher temperatures in zero-field to progressively demagnetize the sample and determine the demagnetization (unblocking) temperature T_D, at which a NRM component is completely removed. The blocking temperature is defined to be the temperature at which the experimental or geological timescale of the (de)magnetization process is longer than the relaxation time of the particles—for SD particles, the two can be related to each other using contour plots of relaxation time versus blocking temperature called nomograms (Néel 1949; Pullaiah *et al.* 1975). Nomograms are widely used to relate blocking temperatures measured in the laboratory to blocking temperatures of remanence acquisition due to geological processes: one first finds the 'laboratory point' described by the measured (un)blocking temperature and the laboratory timescale (typically minutes) and than extends along the corresponding contour to either the geological timescale or the geological temperature of the remanence acquisition process in question (whichever is known) in order to infer the other. Experimental tests of this relationship are generally positive (Dunlop & Özdemir 1993; Dunlop *et al.* 2000; Jackson & Worm 2001), though sometimes anomalously high demagnetization temperatures have been observed (Dunlop 1983; Kent 1985; Kent & Miller 1987); these are often attributed to pseudo-SD (PSD)/vortex and multidomain (MD) grains (Dunlop *et al.* 2000).

Strictly speaking, however, TRM acquisition is a process at non-constant temperature: it occurs during cooling. The cooling rate is known to have a notable effect on palaeointensities, but they also affect unblocking temperatures: The faster a rock is cooled, the lower the apparent blocking temperature (since faster cooling is equivalent to a shorter relaxation time)—the effect is therefore critical for estimation of emplacement/reheating temperatures. York (1978b, a) and Dodson & McClelland-Brown (1980) derived relationships to correct blocking temperatures for the cooling rate r_A. These equations are, however, difficult to test experimentally, since this would require precisely known geological cooling rates, as well as very high-resolution stepwise thermal demagnetization (STD) experiments. Various authors studied the effect of the cooling rate on palaeointensities and the necessary cooling rate corrections (Halgedahl *et al.* 1980; Fox & Aitken 1980; Brown 1963; Ferk *et al.* 2010; Muxworthy & Heslop 2011; Muxworthy *et al.* 2011; Biggin *et al.* 2013; Muxworthy *et al.* 2013; Santos & Tauxe 2019), but few have focused on blocking temperatures.

We recently published a study where, through very accurate continuous thermal demagnetization (CTD) experiments of laboratory induced TRMs and VRMs in a Magnetic Properties Measurement System (MPMS), we were able to experimentally test the heating rate effect on blocking temperatures (Berndt *et al.* 2017). The heating rate is the converse of the cooling rate effect: during CTD, a sample is heated at a heating rate r_D—the faster this rate, the higher the demagnetization temperature T_D. Through these experiments we found slight deviations from the theoretically predicted blocking temperatures, both for experiments involving (1) only the heating rate effect (i.e. CTD of VRMs) and (2) both the heating and the cooling rate effect (i.e. CTD of TRMs), which we suggested to correct empirically for. Here, we present a second set of experiments on the same samples, where we used a modification of the experimental setup to allow for the study of the cooling rate effect in isolation: We experimentally tested (1) the cooling rate effect representative of STD of a TRM, as is important for example for the estimation of volcanic emplacement temperatures (e.g. Paterson *et al.* 2010b) and (2) the relaxation-time–blocking-temperature relationship from the well-known Pullaiah nomograms/Néel theory, as is important, for example for VRM dating studies using STD (e.g. Sato *et al.* 2014). While Berndt *et al.* (2017) studied CTD experiments [relevant, for example, for VRM dating using CTD (e.g. Berndt & Muxworthy 2017)], here we experimentally test the more common STD experiments.

2 THEORETICAL PREDICTIONS

The relaxation time of a rock containing non-interacting SD particles is given by Néel (1949),

$$\frac{1}{\tau} = \frac{2}{\tau_0} \exp\left\{-\frac{\mu_0 M_s H_K V}{kT}\right\}, \tag{1}$$

where τ_0 is the atomic attempt time, μ_0 is the vacuum permeability, M_s is the spontaneous magnetization, H_K is the microscopic coercivity, V is the grain volume, k is the Boltzmann constant and T is temperature. Magnetic blocking occurs when the temperature falls below the point where the relaxation time τ becomes large (relative to the time of either the experiment or of the natural magnetization process). The factor 2 in eq. (1) accounts for blocking in zero external fields (i.e. demagnetization)—for remanence acquisition in a (weak) magnetic field (i.e. acquisition), the factor 2 must be omitted. In this paper, we denote the relaxation time in field (acquisition) by t_A, and in zero field (demagnetization) by t_D. Similarly, acquisition and demagnetization temperatures are denoted by T_A and T_D, respectively. Eq. (1) allows us to relate acquisition and demagnetization times and temperatures (Pullaiah *et al.* 1975):

$$\frac{T_A \ln(t_A/\tau_0)}{1-(T_A/T_C)} = \frac{T_D \ln(2t_D/\tau_0)}{1-(T_D/T_C)}, \tag{2}$$

where T_C is the Curie temperature. In this relation, the temperature variation of M_s and H_K is assumed to be proportional to $\sqrt{1-T/T_C}$, as applicable for (titano)magnetite (e.g. Aharoni 2000). This relationship is well-established for SD grains and has often been confirmed experimentally, but since it assumes constant temperatures, it only applies to VRMs. TRMs, however, are acquired upon cooling at a rate r_A. York (1978b, a), as well as Dodson (1976) and Dodson & McClelland-Brown (1980), derived an expression to relate T_A and r_A to the demagnetization temperature and time T_D and t_D. Berndt *et al.* (2017) introduced the notation of the *effective* relaxation time t_{eff}, which is approximately given by

$$t_{\text{eff}} = \frac{T_A}{r_A}\left(1-\frac{T_A}{T_C}\right) \Big/ \ln\left(\frac{2T_A}{r_A\tau_0}\left(1-\frac{T_A}{T_C}\right)\right). \tag{3}$$

The effective relaxation time can be inserted in place of t_A into eq. (2) to obtain demagnetization times and temperatures of (p)TRMs—it hence plays the role of 'converting' cooling rates r_A to equivalent acquisition times t_A that would create an equivalent remanence at a constant temperature. Both eqs (2) and (3) are tested experimentally in this study.

3 SAMPLES

Two of the same samples used by Berndt *et al.* (2017) were re-used in this study: The Tiva Canyon Tuff sample TC04-12-01K (provided by the Institute for Rock Magnetism, University of Minnesota) and the magnetoferritin sample MFn1 (produced at the Institute of Geology and Geophysics, Chinese Academy of Sciences). The

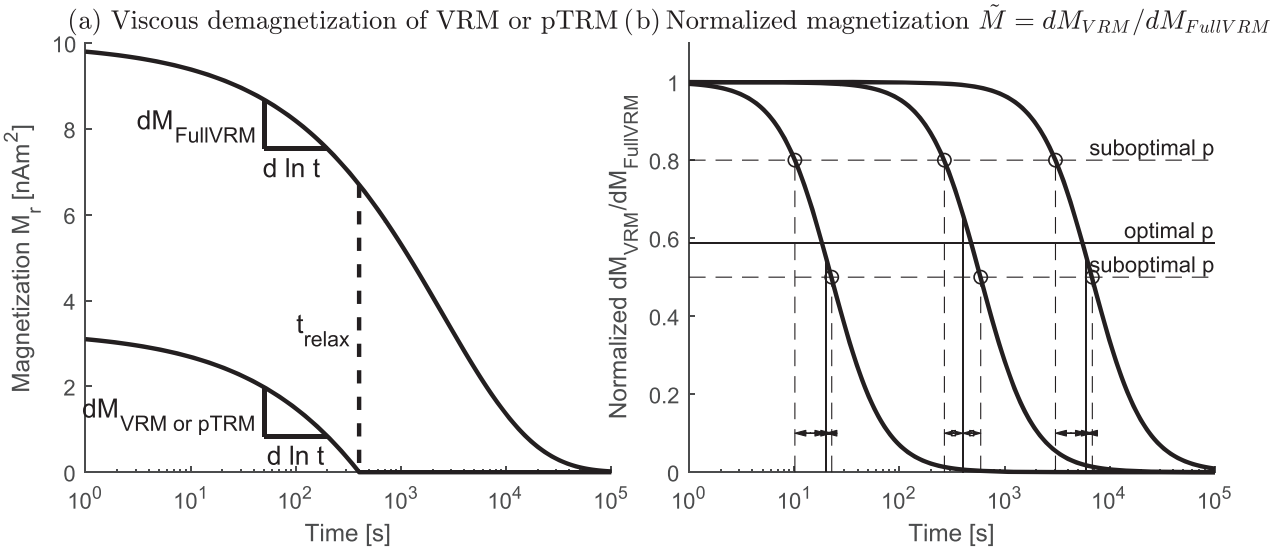

Figure 1. (a) Schematic drawing of the viscous demagnetization protocol. The remanent magnetization curves during viscous demagnetization of a 'full VRM' and partial TRMs/VRMs are shown. 'Full VRM' refers to a VRM of high acquisition temperature and very long acquisition time, such that there is still a significant remanence left at the end of the demagnetization experiment; Partial TRMs/VRMs demagnetize completely during the demagnetization experiment (in this example a 400 s VRM). Note that the shape of the curves depends on the grain size distribution, but are identical before the relaxation time t_D is passed. (b) Schematic drawing of the normalized magnetization $\tilde{M}$ curves (bold lines) for three VRMs with expected demagnetization times of 20 s, 400 s [corresponding to the one in (a)] and 6000 s (solid lines). The parameter p is the percentage of normalized magnetization decay that is used to define the demagnetization time t_D. Dashed lines show different choices of p (arbitrary values for illustrative purposes). For any possible choice of p, there will be some degree of mismatch (arrows) between the expected demagnetization times (solid lines) and measured demagnetization times (dashed lines); p is chosen to minimize the mismatches.

Tiva Canyon sample contains fine-grained low-Ti titanomagnetite, which is mostly super-paramagnetic (SP) at room temperature (Till *et al.* 2011). The titanium content is ca. 10 per cent (TM10, Jackson *et al.* 2006) and grains are highly elongated needles around 15 nm in length (Schlinger *et al.* 1991; Berndt *et al.* 2015). Its Curie temperature was previously determined from thermomagnetic $M_s(T)$ curves to be 471 °C (Berndt *et al.* 2015), which implies a slightly higher Ti-content in this particular sample of ca. TM20. The Verwey transition (Verwey 1939) is suppressed in the samples due to the Ti impurities (Worm & Jackson 1999). First-order reversal-curves (FORC) indicated negligible magnetostatic interactions (Berndt *et al.* 2015).

The magnetoferritin is synthesized through biomimetic mineralization inspired by biological processes in nature, and contains rounded stoichiometric magnetite particles of *ca*. 8 nm diameter, surrounded by a protein shell prevents clustering of particles and reduces magnetostatic interactions (Cao *et al.* 2010, 2014), however, Transmission electron microscopy showed some degree of clustering. It also showed that 90 per cent of the particles are between 6.2 and 11.6 nm diameter and aspect ratios between 1.01 and 1.38 (Berndt *et al.* 2017). The sample is completely SP above 150 K, but stable uniaxial SD at low temperatures—with a saturating field of 200 mT at 10 K (Berndt *et al.* 2017). It was stored sealed and refrigerated since their use by Berndt *et al.* (2017).

4 METHOD

4.1 Viscous demagnetization protocol

Eqs (2) and (3) are experimentally validated in this work: the first provides another confirmation of Pullaiah nomograms for SD grains to relate blocking temperatures in STD experiments to VRMs, and the second to determine cooling rates and hence to enable the use of Pullaiah style diagrams for estimation of emplacement temperatures of (p)TRMs. The experiments presented here closely follow the procedure of Berndt *et al.* (2017), with a specific modification to test the cooling rate effect in isolation—the use of a viscous demagnetization protocol. We first outline the VRM experiments:

(i)First, a (demagnetized) sample is cooled in zero field in an MPMS to a set temperature T_A (33–38 K for the magnetoferritin, 53–58 K for the Tiva Canyon) and a VRM is imparted in a field H_0 of 50 μT for a set time t_A (between 750 and 12 000 s).
(ii)The field is switched off, and the sample is quickly heated or cooled to a target demagnetization temperature T_D (35 K for the magnetoferritin, 55 K for Tiva Canyon).
(iii)The viscous decay of the magnetization is measured in zero field for up to 12 000 s (Fig. 1a)—the '1-step-only' thermal demagnetization.
(iv)The sample is heated up to room temperature and cooled again in zero field to remove any possible remaining remanence.
(v)The process is then repeated at various different acquisition times and temperatures.

From this protocol, T_A, t_A and T_D are known parameters. Hence, to test the validity of eq. (2), t_D must be determined from the viscous demagnetization experiment and compared against the theoretical predictions.

In order to test eq. (3) (to estimate blocking temperatures of pTRMs such as volcanic emplacement temperatures), the first step in the procedure above is modified: First, a (demagnetized) sample is cooled in zero field in an MPMS at a fixed cooling rate r_A (between 0.04 and 0.32 K min^{-1}) to the target demagnetization temperature T_D (35 K for the magnetoferritin, 55 K for Tiva Canyon). At the instant the temperature dropped below the pre-defined acquisition temperature T_A, the 50 μT field was applied to impart a pTRM. The cooling process was continued without interruption till the target

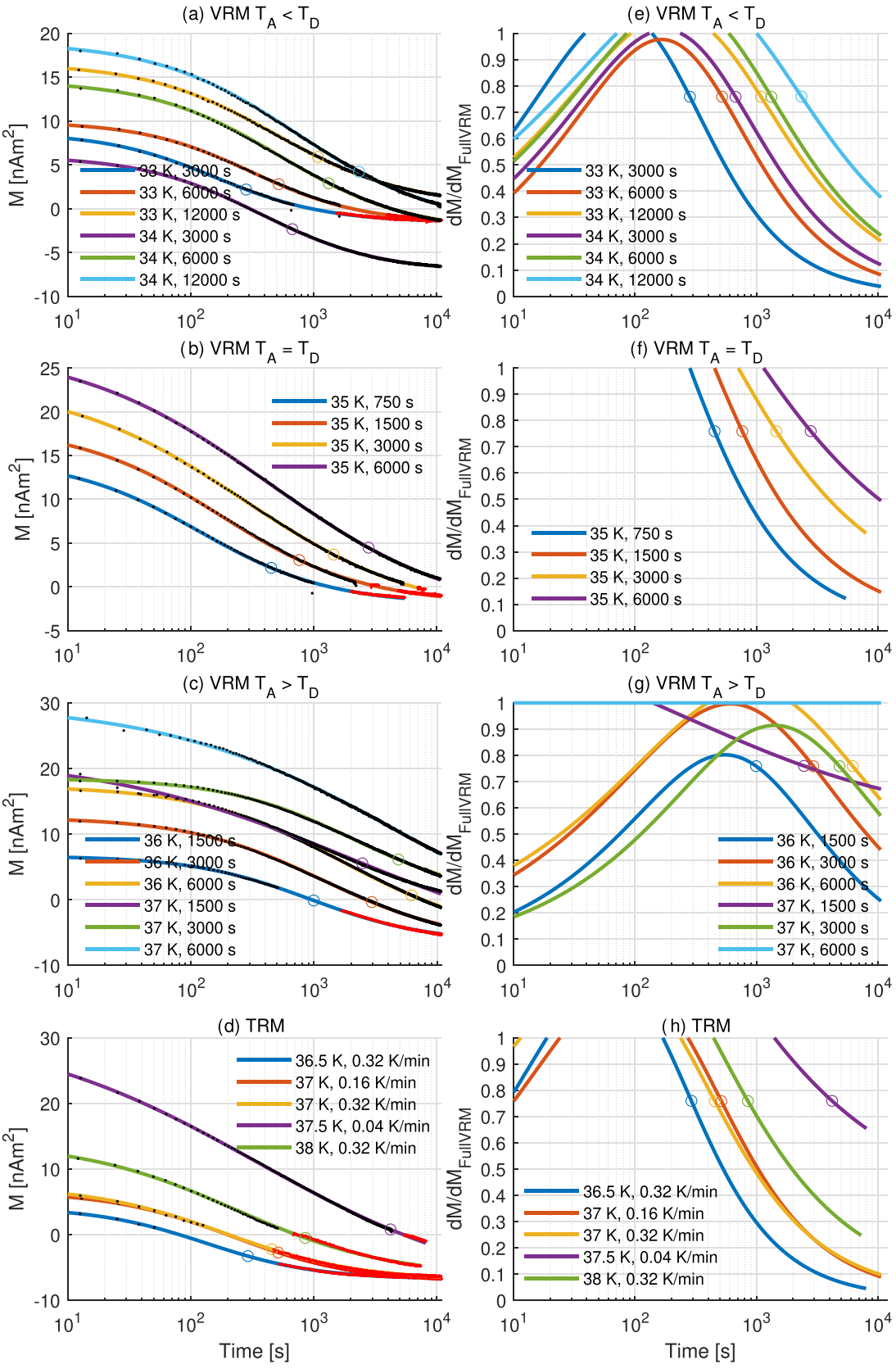

Figure 2. Viscous decay of VRMs (a, b, c) and TRMs (d) for the magnetoferritin sample, all measured at 35 K. (e, f, g, h) Derivatives of viscous decay with respect to the 'full VRM' (37 K, 6000 s). Acquisition temperatures and times/cooling rates are indicated in the plots; black dots indicate raw data; solid lines are smoothed data; red dots indicate raw data corrected for positioning errors of MPMS; circles indicate selected relaxation times as described in the text. For colours, refer to the online version of this paper.

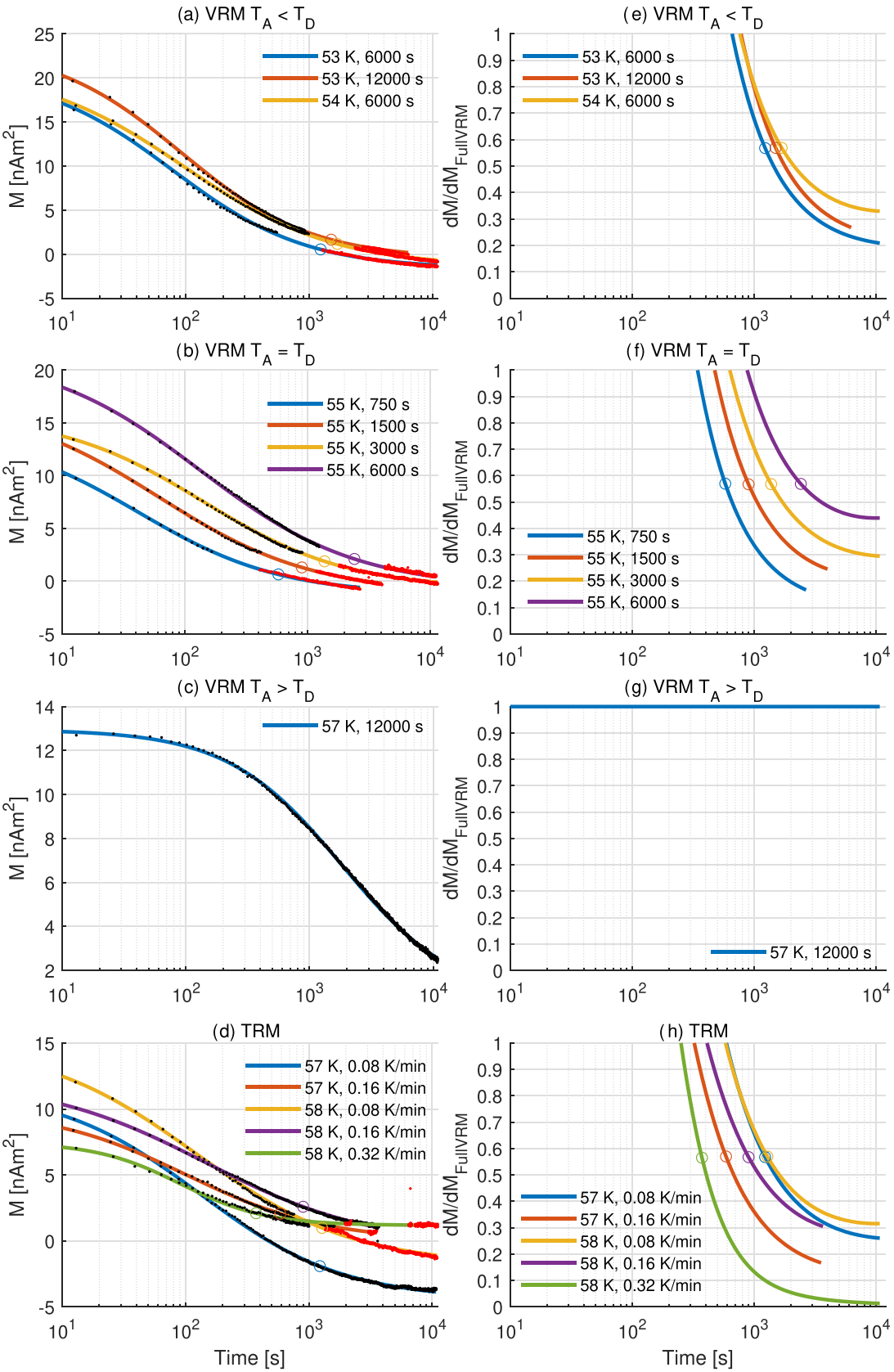

Figure 3. Viscous decay of VRMs (a, b, c) and TRMs (d) for the Tiva Canyon TC04-12-01 sample, all measured at 35 K. Acquisition temperatures and times/cooling rates are indicated in the plots; black dots indicate raw data; solid lines are smoothed data; red dots indicate raw data corrected for positioning errors of MPMS; circles indicate selected relaxation times as described in the text. Derivatives of viscous decay with respect to the 'full VRM' (57 K, 12 000 s) are shown in (e), (f), (g) and (h). For colours, refer to the online version of this paper.

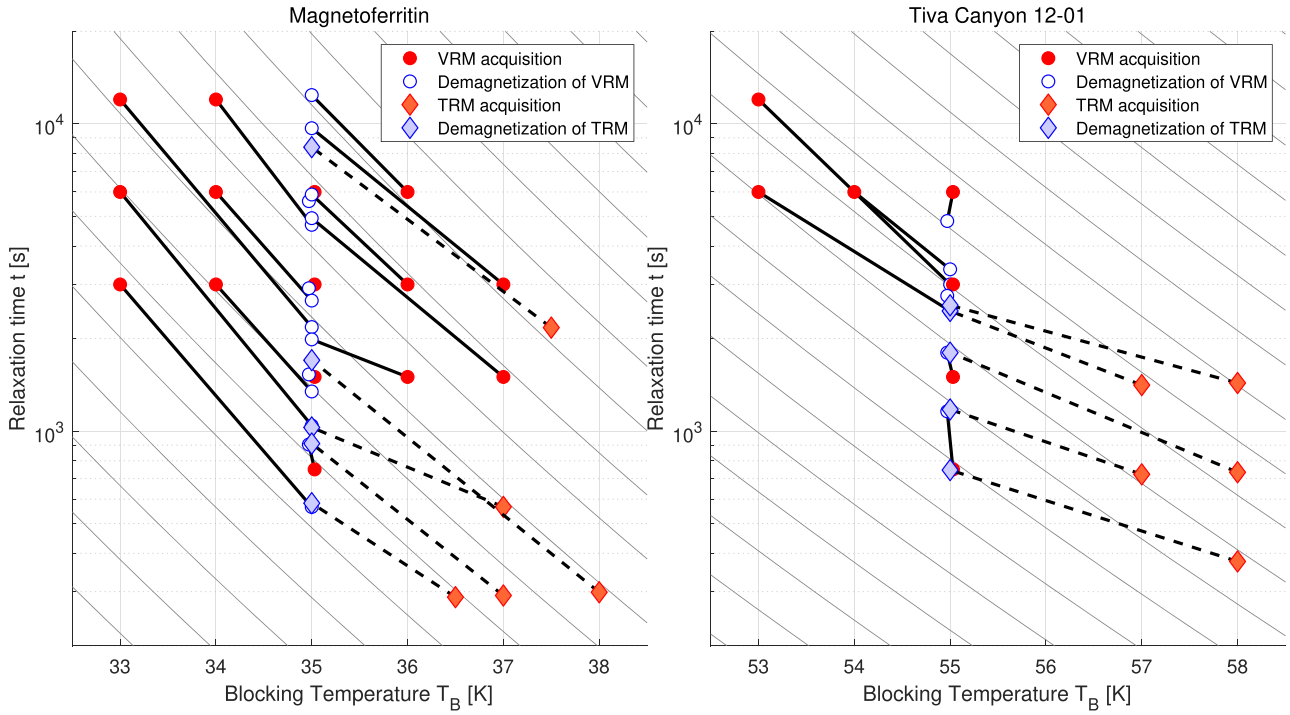

Figure 4. Nomograms of VRMs and TRMs acquired over a given (effective) time t_A and temperature T_A (red) and (viscously) demagnetized at a given demagnetization temperature T_D after a time t_D (blue). Grey lines indicate nomograms after Pullaiah *et al.* (1975) for the best-fitting values of the attempt time τ_0. For colours, refer to the online version of this paper.

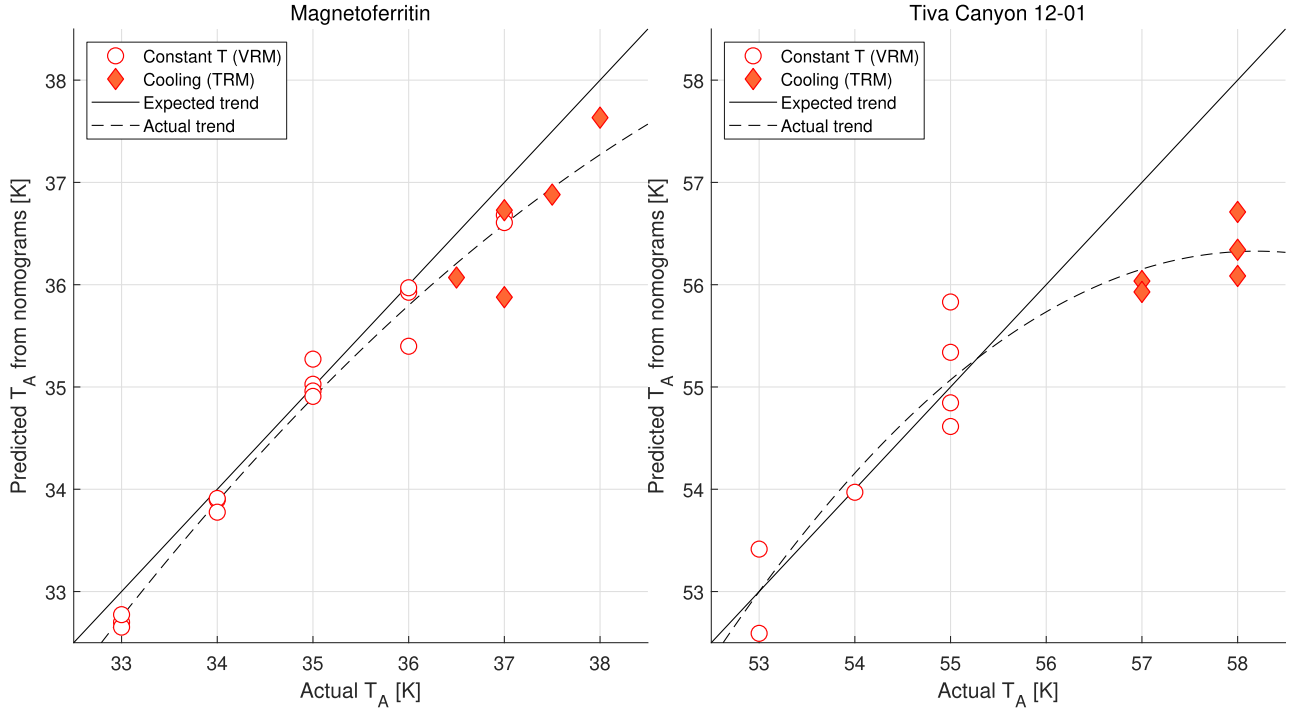

Figure 5. Comparison between the acquisition temperature that would be predicted from the demagnetization temperatures using Pullaiah *et al.* (1975) nomograms (Fig. 4), and the actual acquisition temperature that was used in the VRM/TRM acquisition experiments. Dotted line is a polynomial fit. For colours, refer to the online version of this paper.

demagnetization temperature T_D was reached, at which point the field was switched off, the temperature was kept constant and the viscous decay of the sample was measured as outlined above. For pTRMs, t_A is the effective time t_{eff} of acquisition and is calculated from r_A using eq. (3) and compared against the prediction from eq. (2) using the known T_A, t_A and T_D to test the validity of eq. (3).

The procedure is analogous to classical experimental tests of nomograms that use STD of known VRMs or pTRMs (Dunlop &

Özdemir 1993): in these, the sample is subjected to progressively higher temperatures to demagnetize the VRM/pTRM. At each heating step, the temperature is held constant for a certain amount of time, such that t_D is fixed and known, and the temperature T_D at which the sample is demagnetized, is to be determined from the experiment. The viscous demagnetization protocol effectively uses only one fixed and known temperature step T_D—effectively being a 'one-step-only' STD protocol. By continuously measuring the magnetization, it is possible to determine the relaxation time t_D corresponding to this particular heating step.

Note that in order to achieve a 50 μT field in the MPMS, the copper coils of the MPMS were used to apply a field (the superconducting coils were left off during the whole experiment). The copper coils were carefully calibrated to offset any residual field during the demagnetization experiment and to yield a total 50 μT field during the acquisition experiment.

4.2 Removing grain size dependence

In STD experiments, the demagnetization temperature is defined as the temperature where the remanent magnetization $M_r(T)$ drops to zero. In viscous demagnetization, T_D is held constant and $M_r(t)$ continuously decreases. The exact shape of the $M_r(t)$ curve depends on the grain size and coercivity distributions of the sample. Moreover $M_r(t)$ approaches zero only asymptotically. Hence, an exact definition is needed to determine t_D. Based on the approach by Berndt *et al.* (2017), the procedure is illustrated in Fig. 1: First, we consider the most stable VRM of our set of experiments and call it a 'full VRM'. Acquired at a temperature $T_{A,full}$ (37 K for the magnetoferritin, 57 K for Tiva Canyon) for a long time $t_{A,full}$ (6000 s for the magnetoferritin, 12 000 s for Tiva Canyon), this VRM is sufficiently stable that it did not completely demagnetize over the course of the viscous demagnetization over the following 12 000 s. Therefore, the demagnetization curve $M_{FullVRM}$ only approaches zero asymptotically, as schematically indicated in Fig. 1(a). The procedure is analogous to that used by Berndt *et al.* (2017), in which the samples were demagnetized thermally (i.e. continuous heating), rather than viscously, such that Fig. 1 would show temperature rather than time on the x-axis.

Next, the VRM and pTRM experiments described above are carried out, yielding various viscous demagnetization curves, $M_{VRM}(t)$ or $M_{pTRM}(t)$, respectively, each of which with T_A and/or t_A smaller than T_D and/or t_D, respectively. Consequently, the VRMs/pTRMs do completely demagnetize over the course of the experiment, as indicated in Fig. 1a. Before the VRM/pTRM is completely demagnetized, the shape of $M_{VRM}(t)$ or $M_{pTRM}(t)$ is still dependent of the grain size/coercivity distribution, but is the same as $M_{FullTRM}(T)$, since the exact same grains are being demagnetized. After the VRM/pTRM is completely demagnetized, $M_{VRM}(t)$ or $M_{pTRM}(t)$ should obviously equal zero. Therefore, one can define the 'normalized magnetization' $\hat{M}$ as the ratio between the derivative of the VRM or pTRM demagnetization curves and the derivative of the full VRM, that is

$$\hat{M} = \frac{dM_{VRM\,or\,pTRM}/d\ln t}{dM_{FullVRM}/d\ln t}, \tag{4}$$

which should be close to one for $t < t_D$ and close to zero for $t > t_D$ (Fig. 1b). More mathematically, if the grain size distribution is given by $f(V)$, and $n(V)$ is the net proportion of grains of volume V that are magnetized along the field direction,

$$M_{FullVRM} = \int M_s V f(V) n_{FullVRM}(V)\, dV, \tag{5}$$

and

$$M_{pTRM\,or\,VRM} = \int M_s V f(V) n_{pTRM\,or\,VRM}(V)\, dV, \tag{6}$$

and therefore

$$\hat{M} = \frac{dM_{pTRM\,or\,VRM}}{dM_{FullVRM}} = \frac{n_{pTRM\,or\,VRM}}{n_{FullVRM}}. \tag{7}$$

Note that, while each of the magnetizations (VRM, pTRM, full VRM) depends on the grain size distribution, the normalized magnetization $\hat{M}$ does not depend on the grain size distribution.

4.3 Determination of the relaxation time t_D

Before taking the derivatives of the $M(t)$ curves, the data was smoothed through a best-fitting logistic function. While $\hat{M}$ should theoretically be a step-function, in practice the curve is smoothed out, due to the statistical nature of (un)blocking (Fig. 1b). To determine the relaxation times t_D from these, one has to choose a point where $\hat{M}$ decayed to a proportion p of its initial value; p is chosen as a best-fitting parameter that minimizes the mismatch between the 'measured relaxation times t_D' and the 'expected relaxation times' as obtained from eqs (2) and (3) for the experiments with $T_D = T_A$ (for which, consequently, $t_D = t_A/2$, *cf.* Berndt *et al.* 2017).

4.4 Determination of the attempt time τ_0

Eqs (2) and (3), and therefore the slope of nomograms, strongly depend on the attempt time τ_0. The attempt time is determined from the VRM data only using a least-squares optimization: Either side of eq. (2) is equal to the blocking volume V_B. Therefore, $\ln(V_B)$ is calculated from T_A and t_A on the one hand, and from T_D and t_D on the other hand. The difference between the two $\ln(V_B)$ is then minimized by (iteratively) adjusting τ_0 until the best fit is found. Using only VRM data for the optimization allows to test the validity of the predictions of the cooling rate effect [i.e. pTRMs, eq. (3)].

4.5 Data correction and rejection criteria

A few of the measured demagnetization curves had to be excluded from the analysis, mostly due to reasons relating to the way the MPMS operates. The MPMS measures magnetic moments by physically moving the sample through a set of superconducting coils and measuring the change in the induced current during this process. The arrangement of the coils gives rise to a characteristic curve of induced current versus sample position with multiple (positive and negative) peaks; a model curve is then fitted to the measured current curve, from which both the magnetic moment and the exact sample position is determined. This procedure is intrinsically problematic for measuring magnetic moments close to zero. In such cases, the amplitude of the induced currents is small and the fitting routine becomes error-prone with respect to both moment and positioning—any incorrect fit in the positioning will lead to an incorrect fit to the magnetic moment. Fortunately, however, this mismatch in positioning tends to occur in a very consistent way—the magnetic moment tends to be offset by a constant value. Much of the data where this happened could therefore be corrected by applying a constant offset to 'match up' incorrectly fitted data to the correctly fitted data. The details of this procedure are described in the Supporting Information, where the complete raw data is also presented. Some of the experiments could not be corrected and were excluded from analyses (also described in the Supporting Information).

Table 1. Summary of fitted parameters. 'CTD': parameters obtained in a previous study using continuous thermal demagnetization (Berndt *et al.* 2017).

Sample		p	τ_0
Magnetoferritin	This study	76 per cent	8×10^{-8} s
	CTD	54 per cent	9×10^{-9} s
TC04-12-01	This study	57 per cent	2×10^{-9} s
	CTD	82 per cent	1×10^{-13} s

5 RESULTS

Figs 2 and 3 show the raw and smoothed demagnetization curves $M_{VRM}(t)$ and $M_{pTRM}(t)$, together with the normalized demagnetization curves $\hat{M}(t)$. The percentages p of the magnetization decay that yielded best fits for the demagnetization temperatures are given in Table 1, together with the best-fitting values of the atomic attempt time τ_0 and are compared to those obtained by Berndt *et al.* (2017). Using these best-fitting values, nomograms are plotted in Fig. 4, along with the acquisition values T_A and t_A and demagnetization values T_D and t_D (demagnetization times are multiplied by two to correct for the zero-field). The magnetoferritin sample shows an excellent fit of the experimental data for VRMs (constant temperature acquisition) with the Pullaiah nomograms, while the Tiva Canyon sample is more noisy. Many of the measured Tiva Canyon demagnetization curves were of low data quality and had to be excluded from the analysis due to reasons outlined in the Supporting Information.

The diamonds in the nomograms (Fig. 4) indicate data for the pTRMs, that is acquisition through cooling, and hence indicate whether or not the cooling rate eq. (3) is experimentally confirmed. Again, for the magnetoferritin sample, the points agree very well with the nomograms, indicating that eq. (3) is appropriate to convert cooling rates to effective acquisition times. For the Tiva Canyon sample, however, the slope of the pTRM lines (dashed lines in Fig. 4 is consistently shallower than the nomograms, which indicates that the measured demagnetization times were shorter than predicted from eqs (2) and (3), or conversely that one would underestimate acquisition times / temperatures when applying the theoretical equations to demagnetization data from stepwise thermal demagnetization experiments. This effect is shown more clearly in Fig. 5, which compares acquisition temperatures that would be predicted by applying the equations to the demagnetization data versus the actual (known) acquisition temperatures. While the predicted T_A agree well with the actual T_A for the magnetoferritin for both VRMs and pTRMs, they are consistently too low (by 1–2 K) for the pTRMs of the Tiva Canyon sample.

6 DISCUSSION

The two studied samples arguably belong to the most ideal (non-interacting SD magnetite) materials that may be encountered in rock magnetism.

The precisely size-controlled nature of the magnetoferritin synthesis might be considered akin to magnetic particles by magnetotactic bacteria, that is magnetosomes, that are able to produce similarly well controlled grain sizes and shapes of magnetite and belong to the most ideal natural samples—though these tend to be strongly interacting. The Tiva Canyon sample is a natural sample, which is widely used as a 'benchmark' sample for its near ideal non-interacting SD behaviour in studies of fundamental rock magnetism. The two samples here can therefore be considered a 'best case' scenario of cooling rate corrections/blocking temperature estimations of natural materials. As was found in the experiments, the synthetic magnetoferritin sample followed the theoretical predictions closely—confirming that the theoretical framework for cooling rate corrections are sound. The Tiva Canyon Tuff, however, followed the theoretical predictions only approximately. In particular, the pTRM experiments showed that the cooling rate eq. (3) underestimated the blocking temperature (or conversely the cooling rate). Possible reasons for this include deviations from ideal non-interacting SD behaviour, presence of small amounts of secondary magnetic minerals, and surface oxidation of grains. Also, even though the Verwey transition is suppressed in (low Ti) titanomagnetite, there is still a relatively sharp increase in M_s around the measured temperature range (Berndt *et al.* 2015, 2017; Worm & Jackson 1999)—multidomain titanomagnetite is known to show anomalous field-cooling, zero-field-cooling and frequency dependent susceptibility behaviour, possibly due to the suppression of thermally activated electron hopping (Carter-Stiglitz *et al.* 2006) that impacts magnetic anisotropy. In our sample, the grain sizes are, however, much smaller than multidomain size; nevertheless, this effect may have impacted the cooling rate behaviour. Additionally, there may be problems related to the experimental execution such as movement of the sample (or grains in the powdered sample) in the measurement holder—such problems, however, would only affect individual experiments and likely not lead to a consistent deviation from theory.

In the study of the heating rate effect in continuous thermal demagnetization experiments, systematic deviations from the theoretical equations were found that had to be corrected for empirically (Berndt *et al.* 2017). For the cooling rate effect studied here, we did not find the need for any empirical correction. Moreover, the attempt time τ_0 for the Tiva Canyon sample was found in this study to be in the range of commonly cited values for magnetite (2×10^{-9} s, *cf.* Berndt *et al.* 2015), while Berndt *et al.* (2017) found a very lower of 1×10^{-13} s (Table 1). A possible reason for the difference between the two studies was the magnitude of the applied field [1 mT in Berndt *et al.* (2017), 50 μT here]. It is therefore possible that fields larger than a few hundred μT cause deviations from the cooling rate equation. Weak fields similar to the one used here are geologically much more relevant, such that the cooling rate equations can be applied.

Finally, our pTRM acquisition experiments exhibit a strong dependence on cooling rate that highlight shortfalls in applying SD cooling rate theory to palaeointensity data from natural samples: Comparing the pTRM acquisition for the magnetoferritin acquired from 37 K at cooling rates of 0.16 and 0.32 K min^{-1}, we find that halving the cooling rate increases the pTRM intensity by ~7 per cent. A similar comparison for the Tiva Canyon Tuff pTRMs acquired from 58 K at cooling rates of 0.16 and 0.32 K min^{-1}, indicates a pTRM increase of ~43 per cent for a halving of cooling rate. A factor 2 change in the cooling rate is only predicted to change the remanence intensity by a factor of ~1–2 per cent (Halgedahl *et al.* 1980). This discrepancy is likely related to the often-overlooked fact that cooling rate corrections are blocking temperature dependent (Dodson & McClelland-Brown 1980): At low T_B the cooling rate effect is enhanced, which might explain the large discrepancies. Combined with the effects of non-linear Newtonian cooling (Yu 2011), this effect might also produce small degrees of curvature in Arai plots.

Although some studies have illustrated large, but variable cooling rate corrections in igneous materials (e.g. Yu 2011; Santos & Tauxe 2019), statistical analyses indicate that most palaeointensity studies from igneous rocks accurately identify a known mean value (e.g. Paterson *et al.* 2010a, 2014). This suggests that the effect of cooling rates are small and contribute to data scatter, or that the typical data selection processes screen out these effects.

7 CONCLUSIONS

In conclusion, the experiments show that the cooling rate correction eq. (3) by York (1978b, a) holds and can be applied to non-interacting SD particles. It does, however, also show that even slight deviations from this ideal case have a potentially significant effect on cooling rate corrections. This has important implications for a number of palaeomagnetic applications:

(i)A direct application of this result is the estimation of emplacement temperatures of, for example pyroclastic deposits (Kent *et al.* 1981; Paterson *et al.* 2010b) and intrusive rocks/dykes (Hyodo *et al.* 1993): These rocks acquire pTRMs upon reheating, the temperature of which can be estimated from unblocking temperatures in stepwise thermal demagnetization experiments. Our results show that these can be obtained from nomograms and the equations by York (1978b, a), but that the samples must be carefully tested for mineralogy (ideally uniform) and domain states (ideally SD).
(ii)Our results show that VRM dating, used to estimate deposition times of flood deposits (Sato *et al.* 2014), glacial moraines (Crider *et al.* 2015), landslides (Smith & Verosub 1994), as well as archaeological constructions (Heller & Markert 1973; Borradaile 1996) from stepwise thermal demagnetization experiments should yield accurate time estimates. The same is true for thermoviscous problems such as inferring either times or temperatures of reheating associated with burial of rocks (Kent 1985; Kent & Miller 1987). These applications appear to be less critically dependent on the presence of ideal non-interacting stoichiometric SD grains.
(iii)For VRM dating using continuous thermal demagnetization (Muxworthy *et al.* 2015; Berndt & Muxworthy 2017), our results suggest that, contrary to Berndt *et al.* (2017), VRM ages obtained from effective demagnetization temperatures should be accurate, too, for magnetic fields of the strength of the geomagnetic field.
(iv)Like other studies (Santos & Tauxe 2019), we found a large variability of the cooling rate effect on palaeointensities, that is T_B-dependent. This highlights the importance of determining the cooling rate effect on palaeointensities on a per-sample basis, rather than solely relying on the theoretical correction.

ACKNOWLEDGEMENTS

This study was supported by a Boya Post-doctoral fellowship funded by Peking University and an Institute for Rock Magnetism (IRM) Visiting Researcher Fellowship to TAB; a National Natural Science Foundation of China (NSFC) grant (no. 41574063) and a Natural Environmental Research Council (NERC) Independent Research Fellowship (NE/P017266/1) to GAP; a NSFC grant (no. 41774076) to CC; and a NSFC grant (no. 41722402) to LC. The IRM is a US National Multi-user Facility supported through the Instrumentation and Facilities program of the National Science Foundation, Earth Sciences Division and by funding from the University of Minnesota. The manuscript benefited from the efforts of Y. Yu and multiple anonymous reviewers. The experimental data as well as the code to to analyse and plot it are freely available on https://github.com/thomasberndt.

REFERENCES

Aharoni, A., 2000. *Introduction to the Theory of Ferromagnetism,* 2nd edn, Oxford Univ. Press.
Berndt, T.A. & Muxworthy, A.R., 2017. Dating Icelandic glacial floods using a new viscous remanent magnetization protocol, *Geology,* **45**(4), 339–342.
Berndt, T.A., Muxworthy, A.R. & Paterson, G.A., 2015. Determining the magnetic attempt time $\tau 0$, its temperature dependence, and the grain size distribution from magnetic viscosity measurements, *J. geophys. Res.,* **120**(11), 7322–7336.
Berndt, T.A., Paterson, G.A., Cao, C. & Muxworthy, A.R., 2017. Experimental test of the heating and cooling rate effect on blocking temperatures, *J. geophys. Int.,* **210**(1), 255–269.
Biggin, A.J., Badejo, S., Hodgson, E., Muxworthy, A.R., Shaw, J. & Dekkers, M.J., 2013. The effect of cooling rate on the intensity of thermoremanent magnetization (TRM) acquired by assemblages of pseudo-single domain, multidomain and interacting single-domain grains, *J. geophys. Int.,* **193**(3), 1239–1249.
Borradaile, G.J., 1996. An 1800-year archeological experiment in remagnetization, *Geophys. Res. Lett.,* **23**(13), 1585–1588.
Brown, W.F., 1963. Thermal fluctuations of a single-domain particle, *J. appl. Phys.,* **34**(1951), doi:10.1063/1.1729489.
Cao, C., Tian, L., Liu, Q., Liu, W., Chen, G. & Pan, Y., 2010. Magnetic characterization of noninteracting, randomly oriented, nanometer-scale ferrimagnetic particles, *J. geophys. Res.,* **115**(B7), B07103.
Cao, C., *et al.*, 2014. Targeted in vivo imaging of microscopic tumors with ferritin-based nanoprobes across biological barriers, *Adv. Mater.,* **26**(16), 2566–2571.
Carter-Stiglitz, B., Moskowitz, B., Solheid, P., Berquó, T.S., Jackson, M. & Kosterov, A., 2006. Low-temperature magnetic behavior of multidomian titanomagnetites: TM0, TM16, and TM35, *J. geophys. Res.,* **111**(12), 1–12.
Crider, J.G., Globokar, D.M., Burmester, R.F. & Housen, B.A., 2015. Unblocking temperatures of viscous remanent magnetism in displaced granitic boulders, Icicle Creek glacial moraines (Washington, USA), *Geophys. Res. Lett.,* **42**(24), 10 647–10 54.
Dodson, M.H., 1976. Kinetic processes and thermal history of slowly cooling solids, *Nature,* **259,** 551–553.
Dodson, M.H. & McClelland-Brown, E., 1980. Magnetic blocking temperatures of single-domain grains during slow cooling, *J. geophys. Res.,* **85,** 2625–2637.
Dunlop, D.J., 1983. Viscous magnetization of 0.04-100 μm magnetites, *J. geophys. Int.,* **74,** 667–687.
Dunlop, D.J. & Özdemir, Ö., 1993. Thermal demagnetization of VRM and pTRM of single domain magnetite: No evidence for anomalously high unblocking temperatures, *Geophys. Res. Lett.,* **20**(18), 1939–1942.
Dunlop, D.J., Özdemir, Ö., Clark, D.A. & Schmidt, P.W., 2000. Time-temperature relations for the remagnetization of pyrrhotite (Fe7S8) and their use in estimating paleotemperatures, *Earth planet. Sci. Lett.,* **176,** 107–116.
Ferk, A., Aulock, F.W.V., Leonhardt, R., Hess, K.U. & Dingwell, D.B., 2010. A cooling rate bias in paleointensity determination from volcanic glass: an experimental demonstration, *J. geophys. Res.,* **115**(B8), B08102.
Fox, J.M.W. & Aitken, M.J., 1980. Cooling-rate dependence of thermoremanent magnetisation, *Nature,* **283,** 462–463.
Halgedahl, S.L., Day, R. & Fuller, M., 1980. The effect of cooling rate on the intensity of weak-field TRM in single-domain magnetite, *J. geophys. Res.,* **85**(80), 3690–3698.
Heller, F. & Markert, H., 1973. The age of viscous remanent magnetization of Hadrian's Wall (northern England), *J. geophys. Int.,* **31**(4), 395–406.
Hyodo, H., York, D. & Dunlop, D.J., 1993. Tectonothermal history in the Mattawa Area, Ontario, Canada, deduced from paleomagnetism and 40 Ar/ 39 Ar dating of a Grenville Dike, *J. geophys. Res.,* **98**(B10), 18001–18010.

Jackson, M. & Worm, H.-U., 2001. Anomalous unblocking temperatures, viscosity and frequency-dependent susceptibility in the chemically-remagnetized Trenton limestone, *Phys. Earth planet. Inter.,* **126**(1), 27–42.

Jackson, M., Carter-Stiglitz, B., Egli, R. & Solheid, P., 2006. Characterizing the superparamagnetic grain distribution f(V, Hk) by thermal fluctuation tomography, *J. geophys. Res.,* **111**(B12), B12S07.

Kent, D.V., 1985. Thermoviscous remagnetization in some Appalachian limestones, *Geophys. Res. Lett.,* **12**(12), 3–6.

Kent, D.V. & Miller, J.D., 1987. Redbeds and thermoviscous magnetization theory, *Geophys. Res. Lett.,* **14**(4), 327–330.

Kent, D.V., Ninkovich, D., Pescatore, T. & Sparks, S. R.J., 1981. Palaeomagnetic determination of emplacement temperature of Vesuvius AD 79 pyroclastic deposits, *Nature,* **290**(5805), 393–396.

McClelland, E.A. & Druitt, T.H., 1989. Palaeomagnetic estimates of emplacement temperatures of pyroclastic deposits on Santorini, Greece, *Bull. Volcanol.,* **51**(1), 16–27.

Muxworthy, A.R. & Heslop, D., 2011. A Preisach method for estimating absolute paleofield intensity under the constraint of using only isothermal measurements: 1. Theoretical framework, *J. geophys. Res.,* **116**(B4), B04102.

Muxworthy, A.R., Heslop, D., Paterson, G.A. & Michalk, D., 2011. A Preisach method for estimating absolute paleofield intensity under the constraint of using only isothermal measurements: 2. Experimental testing, *J. geophys. Res.,* **116**(B4), B04103.

Muxworthy, A.R., Evans, M.E., Scourfield, S.J. & King, J.G., 2013. Paleointensity results from the late-Archaean Modipe Gabbro of Botswana, *Geochem. Geophys. Geosyst.,* **14**(7), 2198–2205.

Muxworthy, A.R., Williams, J. & Heslop, D., 2015. Testing the use of viscous remanent magnetisation to date flood events, *Front. Earth Sci.,* **3,** 1–9.

Néel, L., 1949. Théorie du traînage magnétique des ferromagnétiques en grains fins avec applications aux terres cuites, *Ann. Géophys.,* **5,** 99–136.

Paterson, G.A., Heslop, D. & Muxworthy, A.R., 2010a. Deriving confidence in paleointensity estimates, *Geochem. Geophys. Geosyst.,* **11**(7), 1–15.

Paterson, G.A., Roberts, A.P., MacNiocaill, C., Muxworthy, A.R., Gurioli, L., Viramonté, J.G., Navarro, C. & Weider, S., 2010b. Paleomagnetic determination of emplacement temperatures of pyroclastic deposits: an under-utilized tool, *Bull. Volcanol.,* **72**(3), 309–330.

Paterson, G.A., Tauxe, L., Biggin, A.J., Shaar, R. & Jonestrask, L.C., 2014. On improving the selection of Thellier-type paleointensity data, *Geochem. Geophys. Geosyst.,* **15,** 1180–1192.

Pullaiah, G., Irving, E., Buchan, K.L. & Dunlop, D.J., 1975. Magnetization changes caused by burial and uplift, *Earth planet. Sci. Lett.,* **28,** 133–143.

Santos, C.N. & Tauxe, L., 2019. Investigating the accuracy, precision, and cooling rate dependence of laboratory-acquired thermal remanences during paleointensity experiments, *Geochem. Geophys. Geosyst.,* **20**(1), 383–397.

Sato, T., Nakamura, N., Goto, K., Kumagai, Y., Nagahama, H. & Minoura, K., 2014. Paleomagnetism reveals the emplacement age of tsunamigenic coral boulders on Ishigaki Island, Japan, *Geology,* **42**(7), 603–606.

Schlinger, C.M., Veblen, D.R. & Rosenbaum, J.G., 1991. Magnetism and magnetic mineralogy of ash flow tuffs from Yucca Mountain, Nevada, *J. geophys. Res.,* **96**(B4), 6035–6052.

Smith, R.T. & Verosub, K.L., 1994. Thermoviscous remanent magnetism of Columbia River basalt blocks in the Cascade Landslide, *Geophys. Res. Lett.,* **21**(24), 2661–2664.

Till, J.L., Jackson, M., Rosenbaum, J.G. & Solheid, P., 2011. Magnetic properties in an ash flow tuff with continuous grain size variation: a natural reference for magnetic particle granulometry, *Geochem. Geophys. Geosyst.,* **12**(7), Q07Z26.

Verwey, E. J.W., 1939. Electronic conduction of magnetite (Fe_3O_4) and its transition point at low temperatures, *Nature,* **144,** 327–328.

Worm, H.-U. & Jackson, M., 1999. The superparamagnetism of Yucca Mountain Tuff, *J. geophys. Res.,* **104,** 25 415–25 425.

York, D., 1978a. Magnetic blocking temperature, *Earth planet. Sci. Lett.,* **39,** 94–97.

York, D., 1978b. A formula describing both magnetic and isotopic blocking temperatures, *Earth planet. Sci. Lett.,* **39,** 89–93.

Yu, Y., 2011. Importance of cooling rate dependence of thermoremanence in paleointensity determination, *J. geophys. Res.,* **116**(B9), B09101, doi:10.1029/2011JB008388.

SUPPORTING INFORMATION

Supplementary data are available at *GJI* online.

Figure S1 Raw data of viscous demagnetization plots for sample MFn1. Large dots indicate data corrected for positioning errors, small dots indicate uncorrected raw data. Lines indicate smoothed data (logistic function fit).

Figure S2 Raw data of viscous demagnetization plots for sample TC04-12-01K. Large dots indicate data corrected for positioning errors, small dots indicate uncorrected raw data. Lines indicate smoothed data (logistic function fit).

Please note: Oxford University Press is not responsible for the content or functionality of any supporting materials supplied by the authors. Any queries (other than missing material) should be directed to the corresponding author for the paper.

APPENDIX A

Table A1. List of symbols and acronyms.

Symbol	Explanation
NRM	Natural remanent magnetization
(p)TRM	(Partial) Thermoremanent magnetization
VRM	Viscous remanent magnetization
Full VRM	A VRM acquired over a very long time such that it is not completely demagnetized in any experiment
SP	Super-paramagnetic
SD	Single-domain
MD	Multi-domain
MPMS	Magnetic Properties Measurement System
CTD	Continuous thermal demagnetization
STD	Stepwise thermal demagnetization
FORC	First-order reversal-curves
T_A	Acquisition temperature (blocking temperature in field)
t_A	Acquisition time (relaxation time in field)
T_D	Demagnetization temperature (blocking temperature in zero-field)
t_D	Demagnetization time (relaxation time in zero-field)
$T_{A,\,full}$	Acquisition temperature to impart a 'Full VRM' (37 K for the magnetoferritin, 57 K for Tiva Canyon)
$t_{A,\,full}$	Acquisition time to impart a 'Full VRM' (6000 s for the magnetoferritin, 12 000 s for Tiva Canyon)
T_C	Curie temperature
t_{eff}	Effective relaxation time (for continuous cooling or heating at rate r)
τ_0	Atomic attempt time
r_A	Cooling rate of TRM acquisition (in field)
$M_r(T)$	Remanent magnetization as a function of temperature
$M_r(t)$	Remanent magnetization as a function of time
$M_s(T)$	Spontaneous magnetization
$M_{VRM}(t)$	Remanent magnetization of a VRM measured over time t
$M_{pTRM}(t)$	Remanent magnetization of a pTRM measured over time t
$M_{VRM\,or\,pTRM}(t)$	Either $M_{VRM}(t)$ or $M_{pTRM}(t)$
$\hat{M}$	Normalized magnetization defined through the differential of the remanent magnetization over the differential the full VRM
H_0	Applied magnetic field
$f(V)$	Grain size distribution
$n(V)$	Net proportion of grains of volume V magnetized along the field direction
V_B	Blocking volume
p	Proportion of the initial magnetization at which the sample is considered demagnetized